Desalination 539 (2022) 115954

Contents lists available at ScienceDirect

Desalination

journal homepage: www.elsevier.com/locate/desal

Hybrid NF and UF membranes tailored using quaternized polydopamine for enhanced removal of salts and organic pollutants from water

Roqaya A. Ismail [a], Mahendra Kumar [a], Noman K. Khanzada [b], Navya Thomas [a], Nurshaun Sreedhar [a], Alicia Kyoungjin An [b], Hassan A. Arafat [a,*]

[a] Center for Membrane and Advanced Water Technology, Khalifa University, P.O. Box 127788, Abu Dhabi, United Arab Emirates
[b] School of Energy and Environment, City University of Hong Kong, Tat Chee Avenue, Kowloon, Hong Kong

HIGHLIGHTS

- Quaternized polydopamine (QSiPD) nanohybrid was synthesized and well characterized.
- QSiPD was used as a filler in PES UF and NF membranes made by NIPS process.
- 2 wt% QSiPD hybrid membrane (UF2) reported 53 % increase in water flux.
- Hybrid NF membranes exhibited significant rejection of both mono and divalent salts.
- The modified membranes exhibited superior antibacterial properties.

ARTICLE INFO

Keywords:
Nanofiltration
Ultrafiltration
Quaternized polydopamine
Nanohybrid
Antifouling

ABSTRACT

In this work, a quaternized polydopamine (QSiPD) nanohybrid was synthesized via condensation reaction between the silicon hydroxyl moieties of the hydrolyzed QSiP and hydroxyl moieties of polydopamine (PDA) and applied for the first time as a single additive to Poly(ether sulfone) (PES) ultrafiltration (UF) and loose nanofiltration (NF) membranes made via non-solvent induced phase separation (NIPS). QSiPD was added at a maximum loading of 8 and 20 wt% in UF and NF membranes, respectively. The nanohybrid material and membranes were thoroughly characterized. The hydrophilicity, surface charge, and pore structures of the hybrid membranes were progressively tuned with the increase of the QSiPD loading. The UF membrane water permeability of the membrane with 2 wt% QSiPD was as high as ~559 L m^{-2} h^{-1} bar^{-1}. The hybrid UF membranes also exhibited superior antifouling activity with a BSA rejection rate of ~99 % uncompromised by the high membrane flux. The hybrid NF membranes showed significant rejection (45–67 %) of several monovalent (NaCl) and divalent ($CaCl_2$, $MgSO_4$, Na_2SO_4) salt solutions and an outstanding rejection of Congo red dye (>99.9 %). Furthermore, both hybrid UF and NF membranes showed a strong antibacterial activity against *E. coli*.

1. Introduction

In addition to the ability of ultrafiltration (UF) membranes to remove high molecular weight organics and to reduce the overall microbial content of surface and wastewater, UF has also emerged as a pretreatment process of seawater in desalination plants [1]. Nanofiltration (NF) membranes, on the other hand, are capable of removing di-valent inorganic salts from saline water during desalination and also other small molecular weight organic substances from surface and wastewater [2]. Both processes, like all membrane processes in general, are susceptible to membrane fouling/biofouling.

Membrane biofouling mitigation approaches can be categorized into two major types: “defending” and “attacking” strategies [3]. Modified membranes that possess improved resistance against the adhesion of biomolecules follow classic “defending” mechanism which can be developed through the incorporation of hydrophilic additives that tend to lower the interaction of hydrophobic biofoulants (i.e., proteins) [4]. Examples of materials that follow defending mechanism approach are

* Corresponding author.
E-mail address: hassan.arafat@ku.ac.ae (H.A. Arafat).

https://doi.org/10.1016/j.desal.2022.115954
Received 26 April 2022; Received in revised form 29 June 2022; Accepted 30 June 2022
Available online 13 July 2022

inorganic additives [5,6], Polyethylene glycol (PEG) [7], and polydopamine (PDA) [8,9]. Previous research shows that hybrid membranes with inorganic additive loadings >0.2 wt% demonstrate poor salt rejection at high feed pressure [5,6], while additive loading above 2 wt % causes agglomeration and defects in hybrid UF membranes. Consequently, water permeability and/or selectivity of hybrid membranes deteriorates with increased loading of inorganic additives [10,11]. Nonionic protein-repellent PEG-based materials are often applied as a hydrophilic membrane additive. However, PEG molecules have shown to be inefficient at inhibiting bacterial adhesion and proliferation [4,12], and not suitable for long-term application as they are prone to oxidative degradation [4]. Contrary to PEG & inorganic particles counterparts, PDA-based modification has better stability [15], and can be strongly coupled with diverse materials, representing an outstanding antifouling agent for membrane modification [16]. PDA has also proved to enhance the compatibility and interaction of filler particles within the hydrophobic polymer matrix at even high loading percentages with sealed structural defects [13]. PDA incorporation has also shown to improve membrane fouling resistance against several organic foulants (e.g., humic acid, bovine serum albumin etc.) [14]. Although modified antifouling hydrophilic surfaces can be generally classified as "defending" mechanism against biofouling [4,17,18], sustained bacterial resistance cannot be guaranteed without a compromise in membrane performance.

The "attacking" mechanism entails membrane modifications that have the ability to kill and inhibit bacterial growth, such as silver nanoparticles [19], quaternary ammonium groups (QAC) [20], and antibiotics [21]. Yet, bacterial surface that possess attacking mechanism suffer from the buildup of dead bacterial cells over the surface, concealing the membrane's functional groups which could later impair their antibiofouling effect [4].

In order to prevent the shortcomings of both approaches, researchers have suggested to integrate both antibiofouling strategies so that the modified membrane will have a bifunctional surface with non-adhering & bactericidal activities. Surface functionalization with AgNP and PEG polymer has resulted in a modified bifunctional surface that has the capacity to kill and repel bacterial cells simultaneously [22]. Lienkamp et al. developed a modified biofouling resistant surface by combining the non-adhering property of zwitterionic polymers and the antibacterial activity of antimicrobial peptides (AMPs) [23]. These novel materials have exhibited promising results but the modified membranes have not yet achieved an improvement in water purification [4]. Therefore, further efforts are required to find more effective and reliable hybrid materials that are capable of killing bacteria with no compromise in membrane's water separation performance. This effect could be anticipated if the PDA and quaternary ammonium compound can be combined, which has only been adopted in the literature for applications other than water purification [24].

In a recent study, we used quaternized polydopamine (QSiPD) to functionalize rGO to enhance the compatibility of GO-based nanohybrid material within the PES polymer matrix, which resulted in a remarkable improvement in the antifouling and antibacterial activity of the modified UF membrane [25]. However, it was not possible to achieve a defect-free membrane without severe agglomeration at QSiPD-rGO loading higher than 8 wt%. And, since the potential of QSiPD as a stand-alone filler has not been studied previously, we explored in this work the impact of incorporating QSiPD nanohybrid as a single well-dispersed, polymer-based additive in Poly (ether sulfone) (PES) UF and NF membranes, and demonstrated that this can be accomplished at high loadings, up to 20 wt% in NF membranes. UF and NF membranes with QSiPD loadings above 8 wt% and 20 wt%, respectively, suffered from impaired pore structures and were thus excluded from the study. We hypothesized that the water attracting moieties in the QSiPD nanohybrid, like phenolic —OH and —NH, would improve the membrane's hydrophilicity and water flux, while the quaternary ammonium moieties would induce high selectivity and antibacterial capabilities. The significant improvement in membrane's surface hydrophilicity, pore structure, and charge density facilitated the fouling resistance of UF hybrid membranes against BSA protein, while enhancing the salt removal capacity of NF membranes.

2. Experimental

2.1. Materials

Poly (ether sulfone) (PES; MW: 58 kDa) was procured from Goodfellow Co., United Kingdom. Prior to use, PES polymer was dried in a vacuum oven at 100 °C for 12 h. Dopamine hydrochloride (Dopa. HCl), 3-aminopropyl triethoxysilane (APTES; 99 %), glycidyl trimethylammonium chloride (GTMAC; ≥90 %), Poly(vinylpyrrolidone) (PVP; MW: 40 kDa), bovine serum albumin (BSA; 66 kDa), methyl pyrrolidone (NMP; 97 %), absolute ethanol (C_2H_5OH; 99.95 %), sodium chloride (NaCl; 99 %), sodium hydroxide (NaOH), concentrated sulfuric acid (H_2SO_4; 96 %), trizma base, magnesium sulphate ($MgSO_4$), sodium sulphate (Na_2SO_4), Congo red dye (CR: λ_{max} = 498 nm), and hydrochloric acid (HCl; 36.5 % *w*/w) were all received from Sigma-Aldrich, Germany. Calcium chloride dihydrate ($CaCl_2.2H_2O$; 98 %) was received from SD Fine Chemicals, India. Sodium dihydrogen phosphate (NaH_2PO_4) and disodium hydrogen phosphate (Na_2HPO_4) were purchased from Merck Chemicals, Germany. All chemicals were used as received with no additional purification. Ultra-pure DI water (Millipore Corp., USA) was used to prepare all the required solutions for this study. The details for the synthesis and characterization of quaternized silica precursor (QSiP) can be found in our recently published paper [25].

2.2. Synthesis of quaternized polydopamine (QSiPD) nanohybrid

Quaternized polydopamine (QSiPD) nanohybrid was synthesized via simultaneous alkaline hydrolysis of QSiP precursor and self-polymerization of dopamine followed by condensation reaction [25,26]. 3.5 g of QSiP solution and 1 g of Dopa. HCl (QSiP:Dopa. HCl; 3.5:1 *w*/w) were added into a flask containing 500 mL of tris buffer solution (50 mM) and 100 mL absolute ethanol. The initial reaction proceeded at room temperature (RT) under stirring speed of 500 rpm for 24 h. Then, the reaction temperature was raised to 70 °C and maintained for 7 h. The reaction mixture was then centrifuged three times at 8000 rpm for 30 min to get rid of residual impurities, followed by vacuum filtration. The recovered QSiPD nanohybrid was dispersed in ethanol until further use in characterization and membrane fabrication.

2.3. Material characterization

High resolution scanning electron microscopy (SEM; FEI Nova NanoSEM 650) was utilized to visualize the surface morphology of the synthesized materials. PDA and QSiPD samples in powder form were dispersed for 30 min in absolute ethanol using a bath sonicator to prepare separate suspensions of PDA and QSiPD at 0.2 mg mL^{-1} concentration. A separate suspension of PDA or QPD was placed onto the surface of prefixed double-sided copper tape on the SEM stubs, then transferred into vacuum oven for drying at 23 °C for 1 h. Then, fixed PDA and QSiPD were sputter-coated with 10 nm layer of gold-palladium metal. The surface images were retrieved using accelerating voltage of 10 kV, spot size of 2.5, and magnification of 1 μm. A field-emission scanning electron microscope (FESEM; Quanta 3D, FIB) was used to determine the elemental composition of the synthesized PDA and QSiPD. Fourier-transform infrared (FTIR-ATR mode) spectrometer (VERTEX, 80/80v, Germany), X-ray Photoelectron Spectroscopy (XPS), and Raman spectroscopy (Witec Alpha 300 RAS) (at 532 nm wavelength), were used to determine the spectra of PDA and QSiPD nanohybrids. FTIR was recorded in the 4000–500 range, and the resolution was ±4 for 128 scans of each sample. Average zeta potential of the PDA and QSiPD nanohybrids (100 μg mL^{-1}, in DI water) was measured using

Table 1
Chemical composition of the dope solution used in the fabrication of pristine and modified membranes.

Membrane	PES (wt%)	PVP (40 kDa) (%)	QSiPD (wt%)[a]	NMP (wt%)
UF0	18	2	–	80
UF1	18	2	1	80
UF2	18	2	2	80
UF4	18	2	4	79
UF8	18	2	8	79
NF0	20	–	0	80
NF15	20	–	15	77
NF20	20	–	20	76

[a] Weight percentage of QSiPD nanohybrid is based on PES weight.

Zeta Potential Analyzer (ZetaPALS, Brookhaven). All measurements were recorded three times to minimize experimental errors. The loading amount of hydrolyzed QSiP on PD was measured via thermal gravimetric analysis (TGA) using thermal analyzer (NETZSCH, Model No. STA 449F3). The TGA analysis was conducted in the range between 0 and 700 °C, at heating rate of 10 °C min^{-1} under nitrogen (N_2) gas flow using a PerkinElmer TGA 4000 thermal analyzer. TGA of PD, was also analyzed under the same experimental condition. The loading amount of QSiP chains in QSiPD nanohybrid was determined from the weight of the residue left at 700 °C for both PDA and QSiPD according to Eq. (1) [27]:

$$Loading\ amount\ of\ QSi\ (\%) = \frac{W_{QPD} - W_{PD}}{W_{PD}} \times 100 \quad (1)$$

where W_{PD} and W_{QPD} are the weight of PDA and QSiPD residues at 700 °C (%), respectively.

2.4. Membranes' fabrication and characterizations

Non-solvent induced phase separation (NIPS) technique was carried out to prepare the pristine and modified membranes [28]. Firstly, fixed amount of QSiPD was dispersed in NMP solvent using bath sonicator (40 kHz) for 1 h. Then, PVP and PES were added consecutively into the NMP-QSiPD solution and dissolved at 60 °C under 300 rpm stirring speed for 3 h. The polymer solution was then left for cooling at RT and the stirring continued for 24 h. Next, the blend solution was ultrasonicated for 15 min to release any trapped air bubbles. The blend solution was then casted onto a nonwoven support (Novatexx 2471 M, Freudenberg, Germany) fixed on a glass plate using a casting knife (Elcometer, UK) with a gap setting of 150 μm. The glass plate was then submerged in DI water coagulation bath. Once the membrane was formed and detached from the glass plate, it was transferred into a fresh DI water bath and left for 24 h to allow for the evaporation of the solvent. Freshly developed membranes were used for characterization and filtration experiments. Modified membranes with 1, 2, 4, and 8 wt% QSiPD nanohybrid were respectively labeled as UF1, UF2, UF4, and UF8, and were applied as UF membranes. Membranes with 15 and 20 wt % QSiPD were labeled as NF15 and NF20, respectively, and were applied as loose NF membranes. For performance benchmarking, pristine membranes without QSiPD were fabricated from NMP, PES and PVP, and labeled as UF0, and NF0. Membranes without support were also fabricated for use in some characterizations by casting the blend solutions on a clean glass plate. The detailed chemical composition of the dope solution used in making each membrane is presented in Table 1. The membrane characterization procedures are described in detail in Section S1, supporting information (SI).

2.5. Performance evaluation of UF & NF membranes

Pure water flux performance was assessed using a dead-end filtration set up (Model No. UHP 4370, Sterlitech Co., USA) as shown in Fig. S1, SI. Before starting the UF experiment, the membrane was compacted by filtering DI water for 30 min at a feed pressure of 2 bar. After compaction, the UF pure water flux was determined by adjusting the feed pressure to 1 bar (300 rpm) and filtering deionized water for 30 min. The weight of the permeate was measured using a digital balance (Ohaus, UK). The following formula was used to calculate the pure water flux (J_w; L m^{-2} h^{-1}) [29]:

$$Jw = \frac{W}{\rho_w \times A \times \Delta t} \quad (2)$$

where W is the weight of permeated water (g), ρ_w is the density of water (1.0 g cm^{-3}), A is the membrane area (m^2), and Δt is the filtration time (h).

The antifouling performance of the UF membranes was evaluated using BSA as a model foulant. Dynamic filtration of a 50 ppm BSA solution was performed for 3 h at 1 bar feed pressure and the flux of the foulant solution (J_{BSA}; L m^{-2} h^{-1}) was calculated. The BSA rejection rate (R_{BSA}%) of the membrane was determined by measuring the foulant concentration in the feed (C^0_{feed}) and permeate ($C^t_{permeate}$) using this following formula [30]:

$$R_{BSA}(\%) = \frac{\left(C^0_{feed} - C^t_{permeate}\right)}{C^0_{feed}} \times 100 \quad (3)$$

After 3 h, the filtration apparatus was cleaned and filled with fresh DI water. The membrane was washed by filling the filtration cell with DI water and keeping it without permeation for 30 min at atmospheric pressure. The filtration step was then repeated, but using 10 mM phosphate buffer solution (PBS) instead of DI water. Then, the filtration cell was emptied and DI water was then filtered through the membrane at 1 bar for 5 min and post cleaning water flux of the membrane was determined (J_{W1}; L m^{-2} h^{-1}). The flux recovery ratio (FRR) was calculated to assess the antifouling capacity of the membrane, using the following equation [29]:

$$FRR(\%) = \frac{J_{w1}}{J_w} \times 100 \quad (4)$$

To confirm the long-term performance stability of UF0 and UF4 membranes, three additional consecutive filtration and cleaning cycles were conducted, as described above. Furthermore, reversible (R_r; %) and irreversible fouling (R_{ir}; %) ratios were also calculated using the following equations, respectively:

$$R_r = \frac{(J_{w1} - J_{BSA})}{J_w} \times 100 \quad (5)$$

$$R_{ir} = \frac{(J_w - J_{w1})}{J_w} \times 100 \quad (6)$$

The filtration performance (pure water flux and salts/dye rejection) of the NF membranes (NF0, NF15, and NF20) was studied using the above-described dead-end filtration system, but at a feed pressure of 4 bar (after pre-compaction for 30 min at 5 bar). The rejection efficiency of the membranes was assessed using four salt solutions (sodium chloride (NaCl), magnesium sulphate ($MgSO_4$), sodium sulphate (Na_2SO_4), and calcium chloride ($CaCl_2$)), all at 1.0 g L^{-1} concentration, and Congo red dye solution at 10 ppm. A conductivity meter (PH/COND 3320, WTW) was utilized to measure the salt concentration of the feed and permeate, whereas the change in dye concentration was measured using a UV–Vis spectrophotometer at 498 nm.

2.6. Biofouling study

An overnight *Escherichia coli* (*E. coli* - DH5α strain) culture was inoculated in a fresh, sterile Luria–Bertani (LB) broth medium of the following composition (g L^{-1}): 10.0 NaCl, 10.0 peptone, 5.0 yeast extract. The inoculated culture medium was then placed on a shaking incubator (KS 4000, IKA) at 150 rpm for 24 h, and the incubation

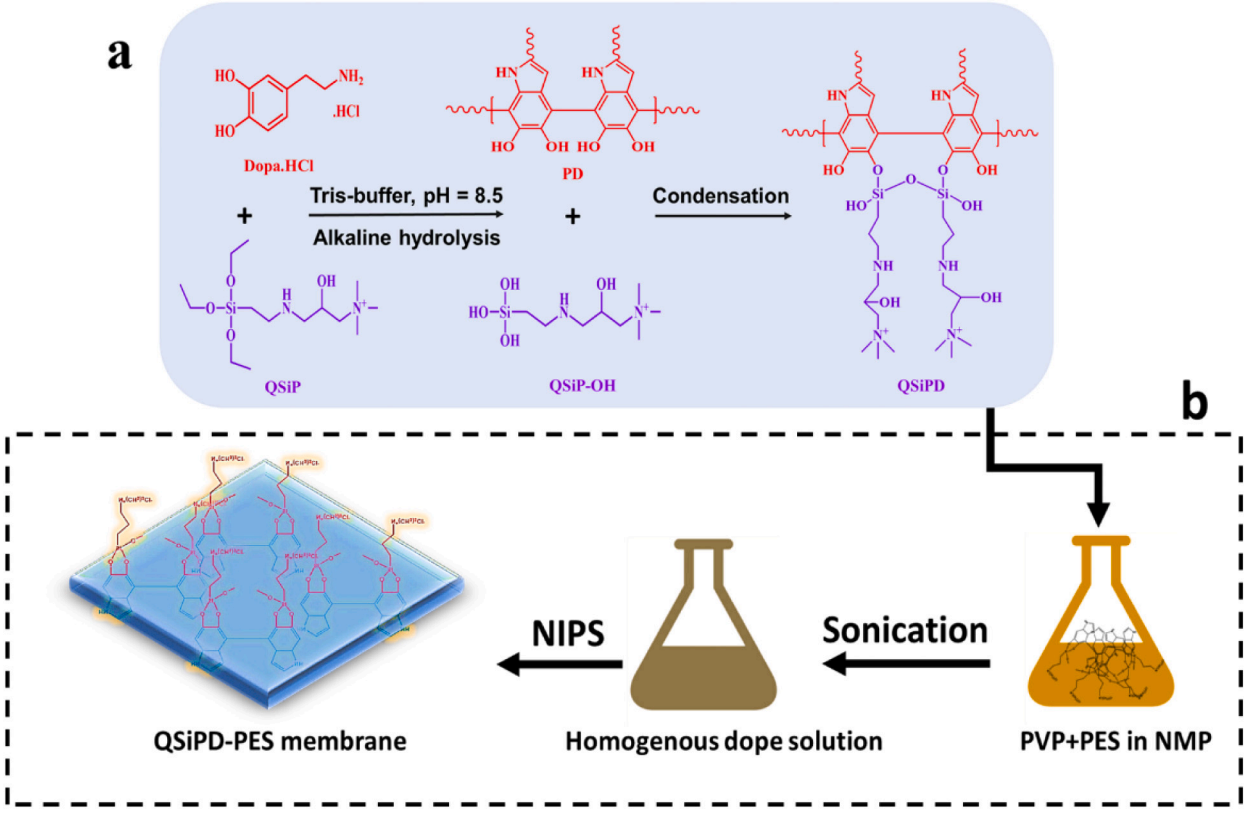

Fig. 1. (a) Schematic of the synthesis route of QSiPD nanohybrid by condensation reaction in a slightly basic medium using hydrolyzed QSiP (QSiP-OH) and self-polymerized polydopamine (PDA), and (b) preparation scheme for QSiPD-PES hybrid membrane.

temperature was maintained at 37 °C. After incubation, the grown bacterial cells were diluted using filter-sterilized 10 mM PBS to reach an optical density (OD_{600nm}) of 0.1 (~10^7 CFU mL^{-1}) [31]. UV–VIS spectrophotometer (UV-1800, Shimadzu, Japan) was used to measure the optical density of the broth after dilution. The bactericidal property of the membranes was studied by placing a small membrane sample (2 cm × 2 cm) into the previously diluted bacterial solutions under an incubation temperature of 37°C and shaking for 1 h. After that, the membrane was rinsed gently with PBS solution to get rid of the loose bacterial cells. Then, the bacterial cells attached on the membrane were harvested from the membrane into 10 mL of 10 mM PBS solution via sonication for 10 min. Post-sonication, the liquid sample was serially diluted (up to 10^6) and spread over the surface of an LB agar plate, then incubated at 37 °C for 24 h. The number of bacterial colonies was then counted and expressed in CFU/mL.

3. Results and discussion

3.1. Formation and characterization of QSiPD nanohybrid

Polydopamine (PDA) nanoparticles were synthesized by oxidative polymerization of dopamine hydrochloride monomers triggered by alkaline conditions using Tris buffer-ethanol mixture [25,32–34]. QSiPD nanohybrid was synthesized via the condensation reaction between the silicon hydroxyl moieties of the hydrolyzed QSiP and hydroxyl moieties of PDA. As a result, quaternized Si chains could be grafted covalently onto the self-polymerized PDA. Subsequently, the crosslinked Si-O-Si linkage was created by the elimination of a water molecule via swift reaction between the hydroxyl moieties of the grafted quaternized Si chains on PDA at 70 °C [25,27,35]. The composition of QSiP and Dopa used in the synthesis of QSiPD nanohybrid was as reported in our

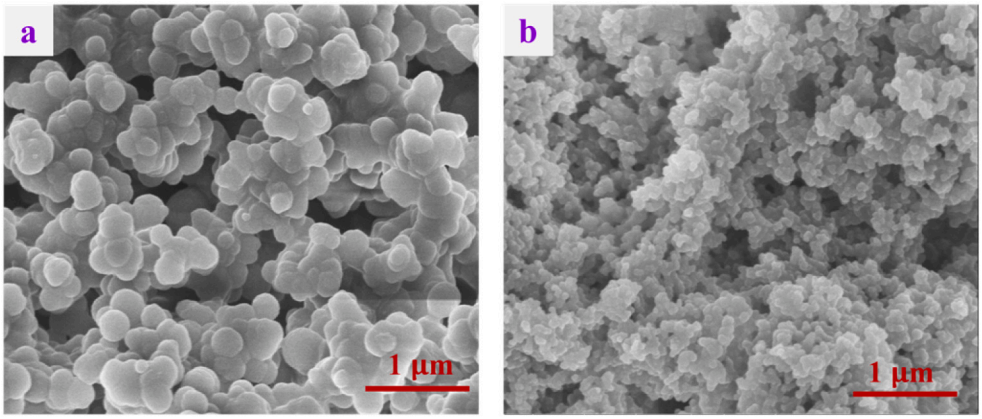

Fig. 2. SEM surface images of (a) PDA and (b) QSiPD.

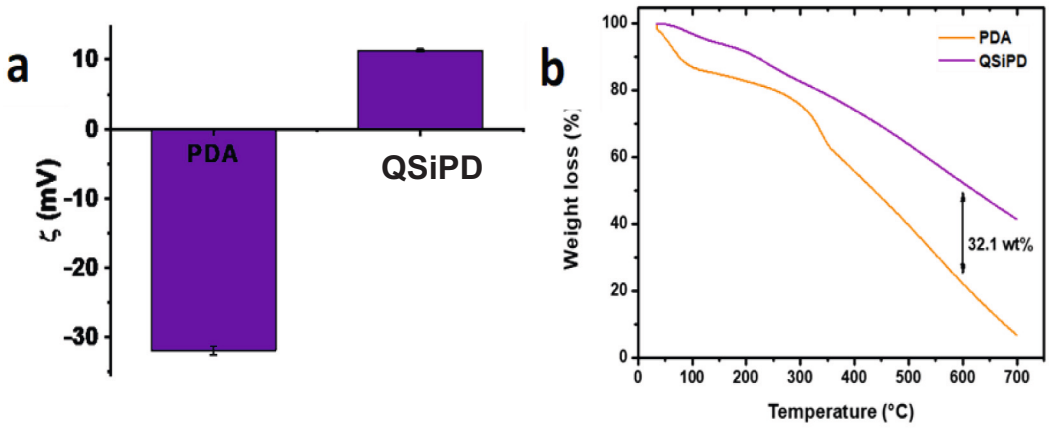

Fig. 3. (a) Zeta potential, and (b) TGA of PDA and QSiPD.

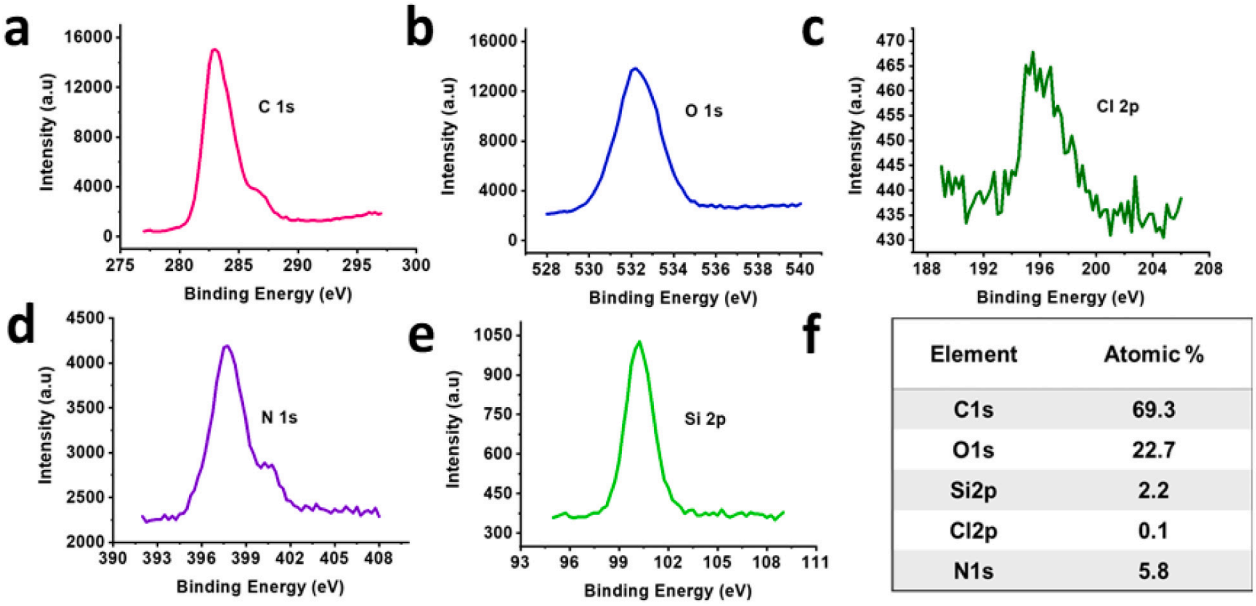

Fig. 4. XPS spectra of: (a) C1s, (b) O1s; (c) Cl2p; (d) N1s; (e) Si2p and (f) elemental composition (%) of QSiPD nanohybrid.

previous work [25]. The synthesis route of QSiPD nanohybrid is depicted in Fig. 1.

The synthesized PDA nanospheres, as shown in Fig. 2 (a), have an average diameter of ~300 nm as formed after 7 h of reaction at pH 8.5. The aggregation of the PDA nanospheres can be attributed to the occurrence of mild solution-phase reaction in a mixture of tris-buffer and ethanol at pH = 8.5 [26]. However, QSiPD (Fig. 2 (b)) exhibited a rougher surface morphology, which could be associated with PDA crosslinking and formation of crosslinked Si—O—Si linkage with the matrix of QSiPD nanohybrid [27,35]. The SEM-EDX spectra of QSiPD nanohybrid further confirms the quaternization with the appearance of new peak for Si (12.29 wt%), in addition to the C and O elements peaks (Fig. S2, ESI).

The surface zeta potential (ζ) of PDA and QSiPD nanohybrid was −31.93 mV and 11.26 mV, respectively (Fig. 3 (a)). The negative surface charge of PDA is attributed to the deprotonation of the phenolic groups (catechol moieties) of PDA at neutral pH [36]. On the contrary, there was a significant alteration in the surface charge of QSiPD nanohybrid. The positive charge of the QSiPD nanohybrid is attributed to the existence of positively charged quaternary ammonium $—N^{+}(CH_3)_3$ groups. These latter groups were more dominant than the deprotonation of phenolic OH moieties during the surface ζ measurements in aqueous solution at neutral pH.

The TGA results (Fig. 3 (b)) indicated that the coated layer of quaternized silica precursor (QSiP) has greatly enhanced the thermal stability of the QSiPD, thanks to the thermally stable Si—O—Si linkages that has formed within the QSiPD nanohybrid. According to the TGA profile, the composition of quaternized silica precursor (QSiP) within the QSiPD nanohybrid at 700 °C is ca. 32.1 wt%.

The synthesized QSiPD nanohybrid was also characterized using FTIR and compared to the spectrum of the PDA nanospheres (Fig. S3, SI). The broad absorption band in the 3000–3500 cm^{-1} region corresponds to the hydroxyl (O—H) and amine (N—H) stretching vibrations of PDA. The sharp peaks at 1602 cm^{-1}, 1506 cm^{-1}, and 1273 cm^{-1} are attributed to the C═C, N—H shearing, and phenolic C—O—H stretching vibrations [25,29,36,37]. Similar, yet broader, peaks were observed in the QSiPD nanohybrid spectra with few additional peaks at 1111 cm^{-1} and 920 cm^{-1} that correspond to Si—O—Si and Si—O moieties, respectively [34,36,38]. Hence, this further confirms that PDA was successfully quaternized with QSiP.

Finally, the surface elemental composition of QSiPD nanohybrid was quantitatively analyzed using XPS to investigate the effect of PDA crosslinking and the formation of crosslinked Si—O—Si linkage with the matrix of QSiPD nanohybrid. The survey scan showed five peaks at 283

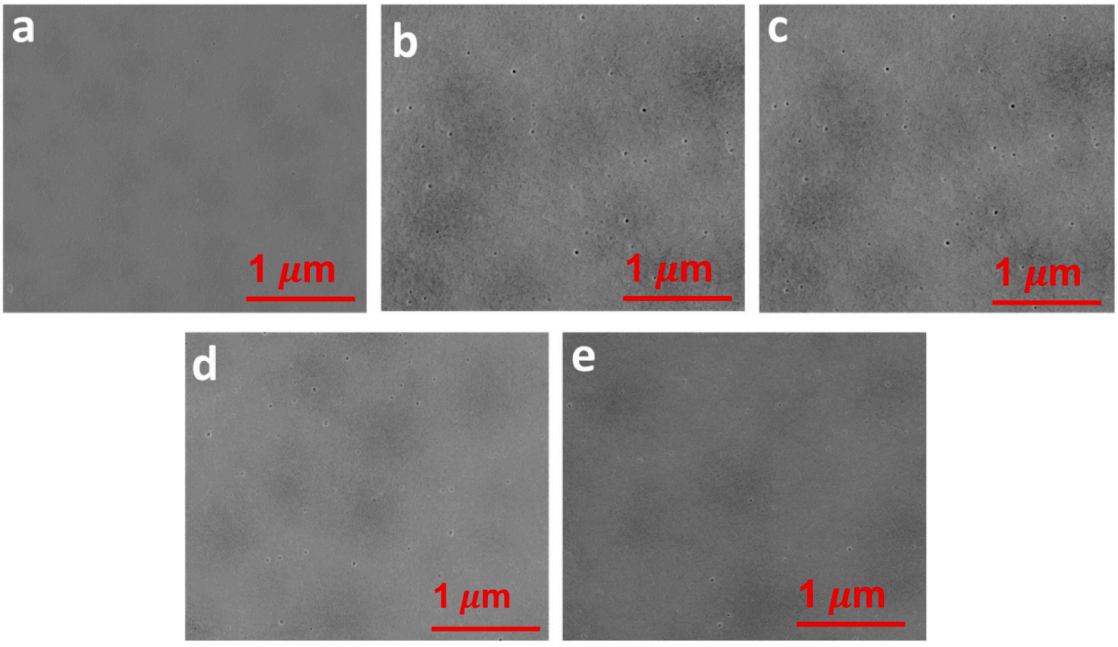

Fig. 5. Top surface SEM images of (a) UF0, (b) UF1, (c) UF2, (d) UF4, and (e) UF8 membranes.

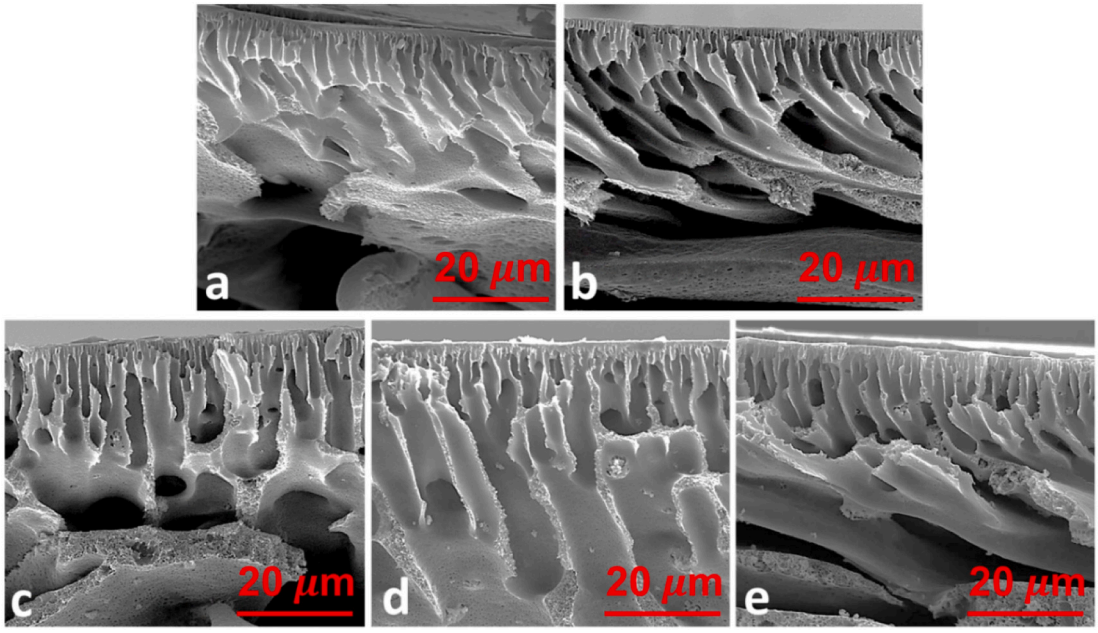

Fig. 6. Cross-sectional SEM images of (a) UF0, (b) UF1, (c) UF2, (d) UF4, and (e) UF8 membranes.

eV, 398 eV, 532 eV, 196 eV, and 100 eV, corresponding to C1s, N1s, O1s, Cl2p, and Si2p, respectively (Fig. 4). These results confirm the presence of QSiP layer on the top surface of modified PDA (QSiPD).

3.2. Formation and morphology of hybrid membranes

A total of five UF membranes (UF0, UF1, UF2, UF4, and UF8) and three NF membranes (NF0, NF15, and NF20) with different QSiPD nanohybrid loadings (up to 8 wt% for UF membranes and 20 wt% for NF membranes) were fabricated through the NIPS method. The top surface and cross-sectional SEM images of the UF membranes are shown in Figs. 5 and 6, respectively. The top surface images reveal that all UF membranes had intact and porous surface, with the pore density of the membranes increasing with QSiPD loading from 1 to 4 wt%, but then significantly decreasing when the nanohybrid filler concentration was increased to 8 wt%. This latter decrease in pore density is attributed to the increase in the viscosity of the dope solution, which led to a delayed exchange between the solvent (NMP) and non-solvent (DI water) during phase separation [25,39,40]. A highly viscous dope solution hinders the escape/evaporation of NMP during the coagulation process, which consequently hinders pore formation and leads to a change in the structural morphology of the pores at the bottom layer.

The cross-sectional SEM images (Fig. 6) show an asymmetric structure composed of a dense layer atop a finger-like porous bottom layer. In contrast to the pristine membrane (UF0), the finger-like pores in the bottom layer became wider and deeper with increasing QSiPD loading,

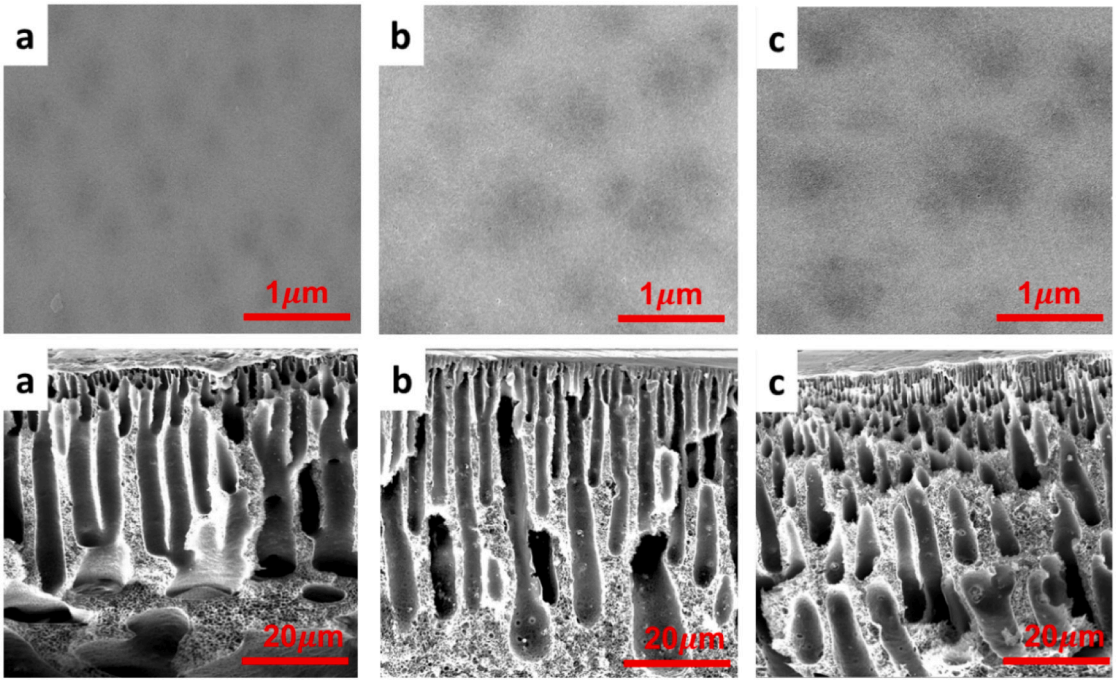

Fig. 7. Top surface SEM images (above) and cross-sectional SEM images (below) of (a) NF0, (b) NF15, and (c) NF20 membranes.

up to 4 wt%. The alterations in the pore structure and size after QSiPD incorporation can be linked to the faster exchange rate between the solvent (NMP) and non-solvent (DI water) during the phase separation process that occurs due to the hydrophilic nature of the QSiPD nanohybrid. This increased hydrophilicity resulted in a thermodynamic instability in the dope solution, thus accelerating phase separation [41,42]. However, the finger-like pores of UF8 membrane were shrunken because of the reduced exchange rate between NMP and DI water, which was influenced by the increased viscosity of the dope solution, as described above [43].

On the other hand, the concentration of PES polymer in the NF membranes has an apparent effect on the membrane structure, which can be also linked to the change in the membrane's pore size and porosity, as shown in Fig. 7. The increase in PES concentration in the dope solution of NF membranes resulted in an increase in the polymer fraction volume during the NIPS process, which consequently led to the formation of a denser top layer. Also, the addition of QSiPD caused insignificant changes in the size of the finger-likes pores of all NF membranes. Yet, the macro-voids at 20 wt% QSiPD appear less uniform with a more polydisperse structure, which can be due to some agglomeration of the QSiPD nanoparticles within the polymer matrix of this membrane.

3.3. Integration of QSiPD into the hybrid membranes

Raman spectra of UF0 and UF4 has affirmed the presence of QSiPD nanohybrid in the fabricated UF membranes (Fig. S4 (a), SI). The absorption bands in 1070 and 1105 cm^{-1} regions correspond to the symmetric and asymmetric stretching vibrations of O═S═O groups. The sharp peak at 1148 cm^{-1} is attributed to symmetric stretching of C—O—C linkages. The absorption band at 1203 cm^{-1} corresponds to a weak asymmetric stretching of the C—O—C linkages. The absorption band at 1600 cm^{-1} in the Raman spectrum of UF4 is attributed to the vibration of phenyl rings and the characteristic G band of QSiPD [25,44]. However, a slight shift in the characteristic peaks linked to the stretching vibrations of O═S═O, C—O—C and phenyl rings was observed, and the peak located at 1596 cm^{-1} appears to be broad in the Raman spectrum of UF4 membrane. This could be ascribed to an additional contribution in the stretching vibrations of phenyl rings by the phenolic moieties of QSiPD nanohybrid within the UF4 membrane matrix. Similar peaks were observed in the Raman spectrum of NF15 membrane (Fig. S4 (b)), which further confirms the presence of QSiPD in the hybrid NF membranes. The incorporation of QSiPD within PES matrix was also confirmed by SEM-EDX (Fig. S5, SI). The appearance of new Si peak in modified UF8 membrane indicated the presence of QSiPD nanohybrid.

The TGA curves of the fabricated membranes are represented in Fig. S6, SI. The inset figure in Fig. S6 (a) shows the variation in weight loss (%) of the membranes in the temperature range of 450 to 650 °C. Three dissimilar stages of weight loss took place during thermal decomposition of all UF membranes in the temperature range of 50–650°C (Fig. S6 (a)). These stages were attributed to: (i) moisture evaporation in the temperature range of 50–120 °C; (ii) pyrolysis of the functional moieties (N—H, phenolic O—H, and $—N^{+}(CH_3)_3$) of hybrid UF membranes in the 300–450 °C range, and (iii) disintegration of PES chains and the crosslinked Si—O—Si linkages of QPD nanohybrid within the hybrid UF membranes matrix at >500 °C [25,45–47]. The thermal decomposition temperature (T_d) of both UF and NF membranes increased with QSiPD loading. T_d of the pristine UF0 (432 °C) was lower than the modified UF1 (537 °C), UF2 (515 °C), UF4 (533 °C), and UF8 (574 °C). Similar observations were noticed for the NF membranes. Hybrid NF membranes (NF15 and NF20) were also more thermally stable than the pristine (NF0) membrane. The incorporation of QSiPD nanohybrid enhanced the thermal stability of the modified membranes due to the strong interaction between the PES polymer and the embedded nanohybrid filler.

3.4. Impact of QSiPD on membrane properties

The observed dynamic water CA of the pristine and modified UF and NF membranes is presented in Fig. 8 (a) and (b), respectively. As the loading of the nanohybrid filler was increased, the CA decreased noticeably, indicating an increase in surface hydrophilicity of the modified membranes. The average static water CA of the virgin UF0 membrane was 80.9°, which decreased to 70.9°, 65.9°, 63.7°, and 60.3° for UF0, UF1, UF2, UF4, and UF8, respectively. A similar trend was

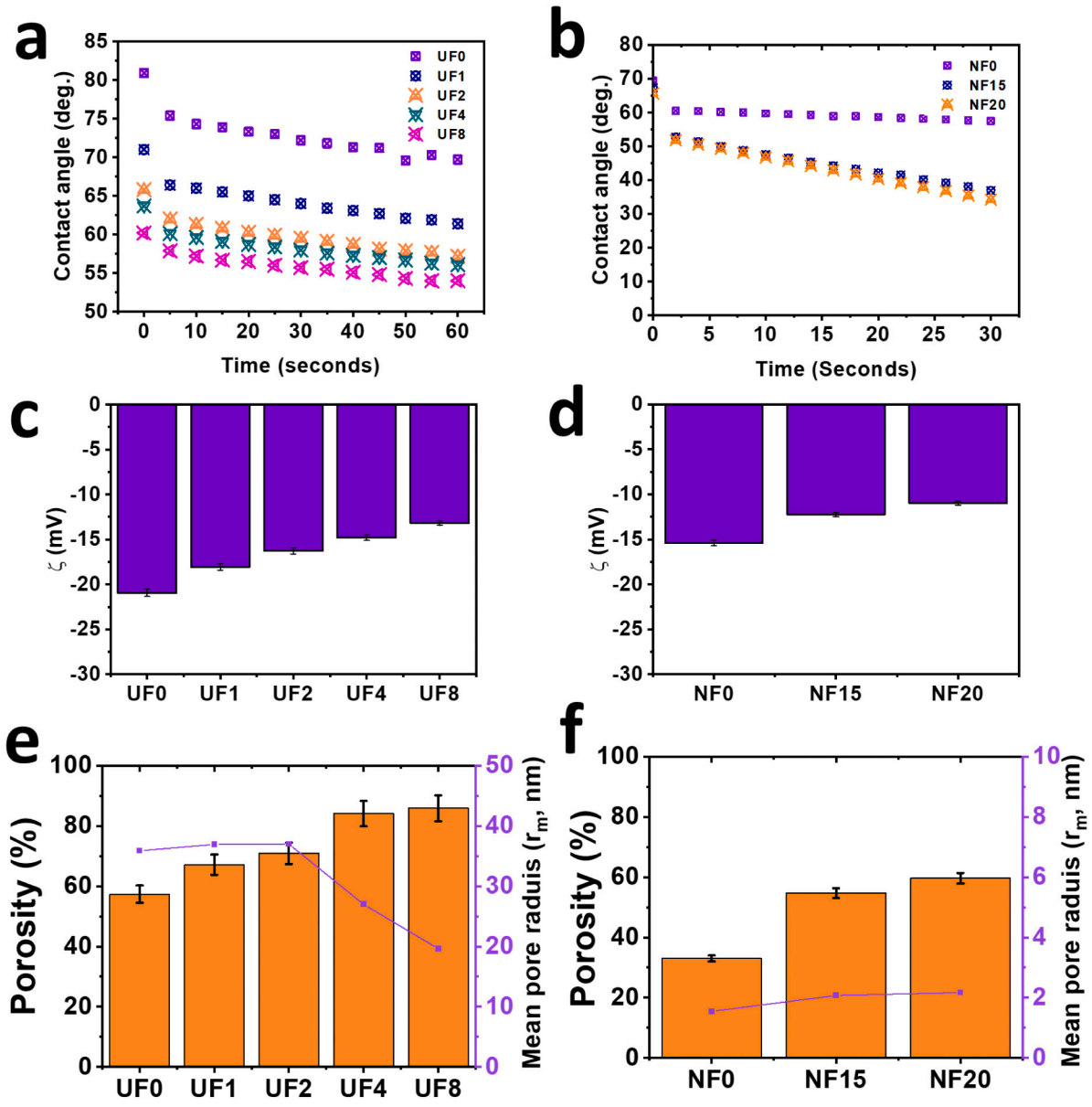

Fig. 8. Dynamic water CA, porosity, and zeta potential, of the UF (a, c, and e, respectively) and NF (b, d, and f, respectively) membranes.

observed for the NF membranes, where the static water CA decreased from 69.4° for NF0 to 67.3° and 65.6° for NF15, and NF20, respectively. The decline in both static and dynamic water CA is linked to the presence of hydrophilic functional groups (e.g., phenolic O—H, N—H and $—N^{+}(CH_3)_3$) on the surface and within the matrix of modified UF and NF membranes. These hydrophilic functional moieties are known to hold and absorb water molecules through ion-dipole and dipole-dipole interactions [44,48]. However, the drop in dynamic CA angle was lower in NF than in UF membranes. This is due to the dense surface layer of the former, which resulted from an increase in the PES fraction volume.

The surface charge of UF and NF membranes was determined as surface zeta potential (ζ) at pH 7. The ζ values of both UF and NF membranes are represented in Fig. 8 (c and d, respectively). The negative ζ values observed in pristine UF0 and NF0 membranes (20.8 and 15.7 mV, respectively) are attributed to the negatively charged anions (OH^{-} and Cl^{-}) adsorbed onto the membrane surfaces during ζ measurements in 10 mM NaCl aqueous solution [25,49]. The surface charge was evidently tuned upon incorporation of the QSiPD nanohybrid into the membranes. The gradual increase in the QSiPD loading led to a systematic increase in the zeta potential, due to the increased presence of positively charged quaternary ammonium groups ($—N^{+}(CH_3)_3$) on the membrane surface, which was intensified in the barrier layer of the hybrid membranes [25,50]. However, the surface charge of hybrid UF and NF membranes could also be partially affected by the formation of negatively charged moieties after the deprotonation of phenolic O—H in the NaCl solution [36].

Both modified UF and NF membranes experienced a gradual increase in their porosity (ε, %) with increased QSiPD loading (Fig. 8 (e & f)). This increase in porosity can be associated with the hydrophilic nature of QSiPD and its tendency to absorb water, resulting in the development of wider water penetration channels during the NIPS process [25,41,51–53]. On the other hand, the porosities of hybrid NF membranes were generally lower than the porosities of hybrid UF membranes due to: i) the absence of pore forming additive, PVP, and ii) the higher concentration of PES and QSiPD in the dope solutions used in the fabrication of NF membranes (Table 1). The latter led to a higher dope solution viscosity and, consequently, slower water-NMP exchange rate during membrane formation. In parallel, the pore size of the modified

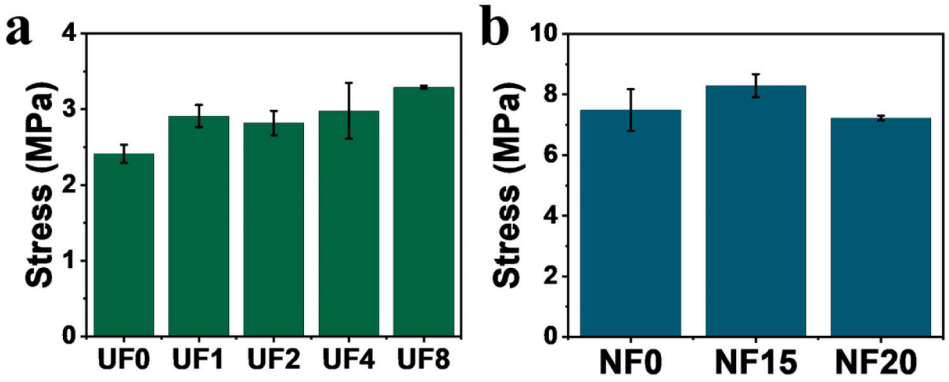

Fig. 9. Tensile stress at maximum load (MPa) of the UF (a), and NF (b) membranes.

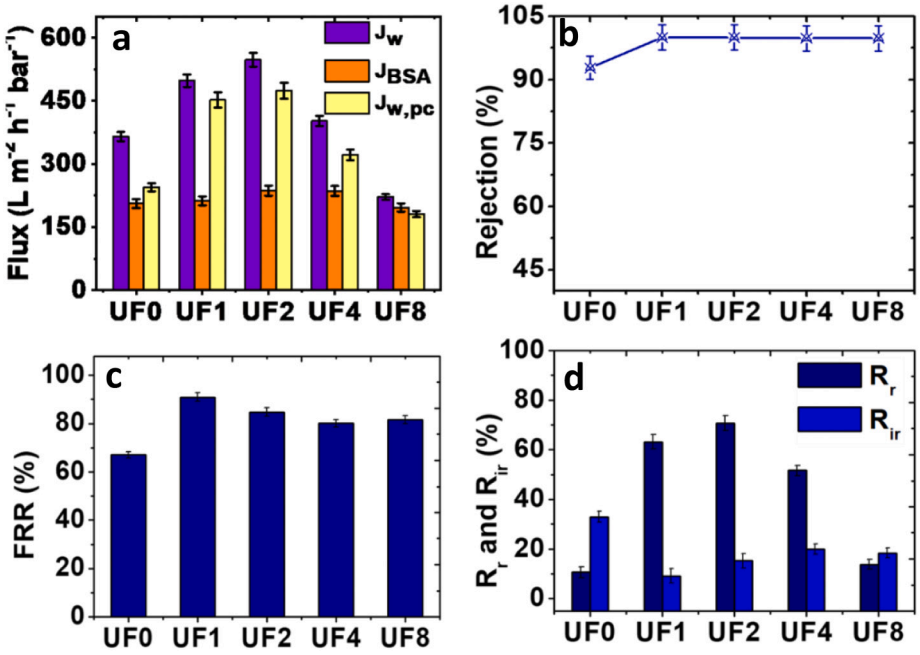

Fig. 10. (a) Pure water flux (J_w), BSA solution flux (J_{BSA}) and post cleaning water flux ($J_{w,\,pc}$) (b) BSA rejection (%); (c) FRR (%) and (d) R_r, R_{ir} (%) of pristine and hybrid UF membranes.

UF membranes increased with QSiPD loading up to 2 wt%, then decreased as seen in Fig. 8 (e). The decrease in the pore size of UF4, and UF8 membranes is also attributed to the increase in the dope solution viscosity, which hindered the widening of the top surface pores during phase separation [54]. On the other hand, all NF membranes exhibited similar pore radius of approximately 2 nm (Fig. 8 (f)), which is well within the NF pore size.

Finally, tensile strength study was performed to probe the effect of QSiPD incorporation on the mechanical properties of PES. The tensile stress at maximum load (MPa) of UF and NF membranes is shown in Fig. 9. The results indicate that the incorporation of QSiPD had a marginal, but favorable, impact on the mechanical strength in UF membranes only. The slight increase in the tensile strength of the hybrid UF membranes could be attributed to an increase in the intermolecular forces between the PES polymeric chains and the embedded QSiPD filler, resulting in an improved overall membrane integrity.

3.5. Influence of QSiPD on membrane performance

3.5.1. Flux and selectivity

The aim of incorporating QSiPD within the membrane matrix is to enhance the membrane surface properties and, consequently, filtration efficiency. Therefore, the modified UF membranes' filtration performance was first tested using BSA solution as a representative organic foulant. Prior to BSA filtration, pure water flux (J_W; L m^{-2} h^{-1} (LMH)) of the pristine and hybrid UF membranes was measured (Fig. 10 (a)). All the modified UF membranes, except UF8, experienced an enhanced water flux compared to the pristine UF0. J_W of UF0 was 365 LMH, which remarkably increased to 498 LMH for UF1, 559 LMH for UF2 and 402 LMH for UF4, but then decreased to 222 LMH for UF8. The improvement in water flux of UF1, UF2 and UF4 is the result of an interplay between increased hydrophilicity, porosity, and mean pore radius and enhanced pore structure of the modified membranes. However, the observed flux drop in UF8 was induced, to a large extent, by the agglomeration of QSiPD within the polymer matrix (Fig. S7), and the compression in the membrane pores and water passage channels. The agglomeration of QSiPD particles can cause pore blockage that affects the water passage that has been described in previous research works [55–57].

The modified UF membranes' potential in filtering and rejecting BSA in a 3 h filtration experiment of a 50 ppm feed solution was evaluated and the findings are presented in Fig. 10. The BSA solution flux (J_{BSA}) results, obtained at the end of the 3 h filtration test, indicate that the

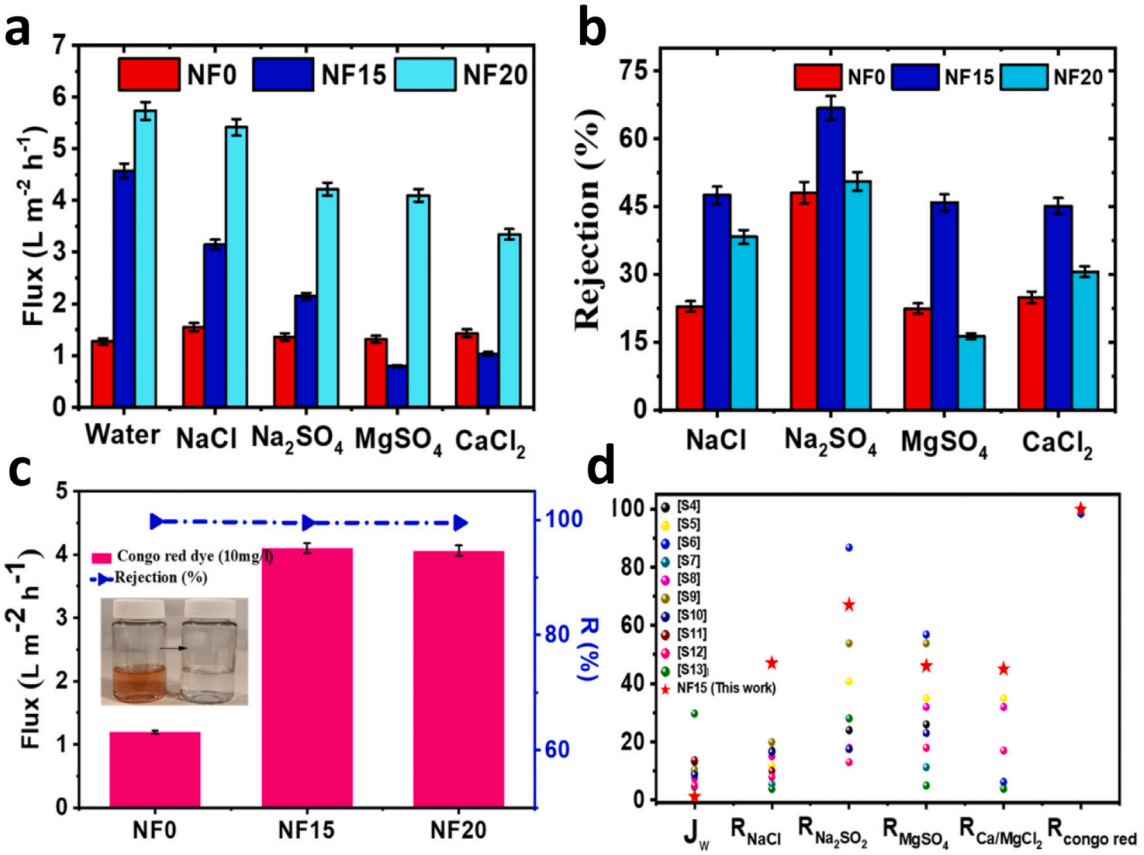

Fig. 11. Pure water flux (J_w), and single salt solutions flux (b) salt rejection, (c) dye flux and rejection capacity of NF membranes, at 300 rpm and 4 bar and (d) Comparison of flux and salt and dye rejections of NF15 with other synthetic MM NF membranes reported in the literature.

accumulation of BSA on the surface of all membranes led to a significant decline in flux. However, UF0 was unable to recover most of its initial water flux after a membrane cleaning step with DI water-phosphate buffer solution, as indicated by the post-cleaning water flux results ($J_{w,pc}$) in Fig. 10 (a). The pristine membrane was not able to recover its initial flux due to the hydrophobic nature of PES that allowed for stronger interaction with BSA protein via electrostatic & hydrophobic forces [58]. On the other hand, the incorporation of QSiPD led to significant improvement in $J_{w,pc}$ and flux recovery rate (FRR) of the hybrid membranes (Fig. 10 (a and c)). The rejection of the BSA (R_{BSA}, %) was also enhanced after QSiPD incorporation, from around 93 % in UF0 to nearly 99 % for all hybrid membranes. This high R_{BSA} occurred even with the higher flux of the hybrid membranes, suggesting a mitigation of the permeability-selectivity trade-off.

The noticeable improvement in the flux and BSA rejection of the hybrid membranes can be explained by the formation of a hydration shell on the membranes surface due to the interdependent effects of hydrophilicity and surface charge, which allowed for easy access of water molecules and prevented the non-specific adhesion of BSA molecules [25,43,44,59,60]. The pore size also contributed to the changes in water flux and BSA rejection. The two fouling resistance components, R_r and R_{ir}, have also confirmed a profound role of QSiPD in suppressing irreversible fouling (Fig. 10 (d)). The least R_{ir} (9.18 %) was observed in UF1, compared to 32.9 % for UF0.

The performance of NF membranes was assessed by testing their ability to separate four salt solutions of different anions and cations (NaCl, $MgSO_4$, Na_2SO_4, & $CaCl_2$) and congo red dye. As presented in Fig. 11 (a), the pure water flux of NF20 (5.7 LMH) and NF15 (4.6 LMH) is nearly 5-fold and 4-fold higher than the pristine NF0 (1.3 LMH), respectively, which is due to the improved hydrophilicity, porosity, and the pore structures of the modified membranes. The modified membranes have also exhibited an improved flux when tested with different salt solutions (except for $MgSO_4$ and $CaCl_2$ in NF15) with salt rejections in the order of Na_2SO_4 > NaCl >$MgSO_4$ > $CaCl_2$ for NF15 and Na_2SO_4 > NaCl > $CaCl_2$ > $MgSO_4$ for NF20. This rejection order of the salts is inconsistent with the previously reported order by positively charged NF membranes [61–65], which could be attributed to the presence of negatively charged hydroxyl moieties on our NF membranes that led to a stronger repulsion forces towards anions than cations. It is well-known that the separation mechanism in NF membranes occurs through sieving (steric) and Donnan exclusion effects and that membrane pore radius and charge play a critical role in this mechanism [66,67]. A positively charged NF membrane can retain positively charged ionic species better, while allowing negatively charged ions to pass more easily through the membrane. However, at 15 wt% QSiPD loading, the rejection of Na_2SO_4 was the highest (~67 %) and the membrane also maintained a relatively high rejections for NaCl (47 %), $MgSO_4$ (46%), and $CaCl_2$ (45%). The rejection of NaCl and $MgSO_4$ was almost similar to NF15, and their moderate retention can be explained by the synergistic effects of size exclusion and Donnan exclusion. However, Na_2SO_4 and NaCl rejections were higher than $MgSO_4$ and $CaCl_2$ and this could be ascribed to the negatively charged hydroxyl moieties on the membrane surface, which provided stronger electrostatic affinity for the divalent cations (Mg^{+2} & Ca^{+2}) than for monovalent Na^+ ions. The drop in the salt rejection potential of NF20 could be due to the presence of surface defects in the skin layer of NF20 or due to the deposition of calcium and magnesium salts on membrane surface during filtration. Also, it is worth noting that the increase in flux didn't cause a loss in the salt rejection capability of the modified membranes (except for $MgSO_4$). This observation can be attributed to the small pore size of the NF membranes and the electrostatic interactions between the positively and negatively charged moieties on the membrane surface on

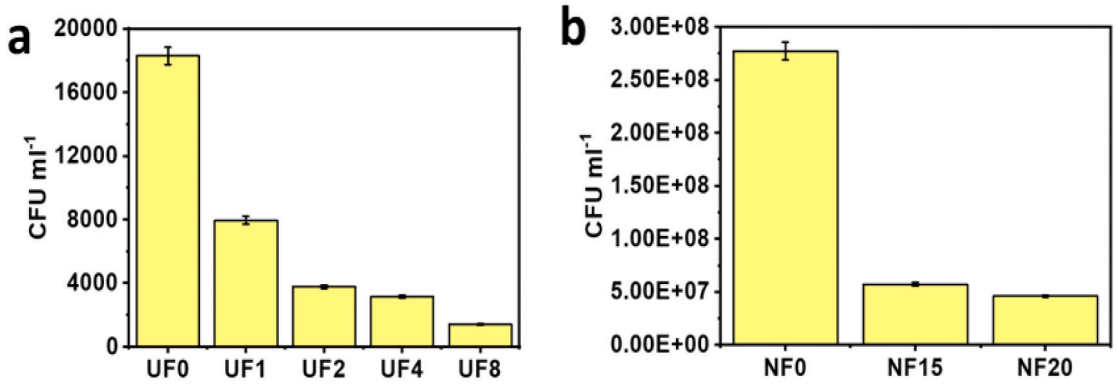

Fig. 12. (a & b) The number of attached bacterial cells on the surface of UF (a) and NF (b) membranes at 37 °C, expressed in CFU/mL.

one side and the salt ions on the other, which helped in achieving high rejection for both mono and divalent salts.

The dye removal performance of the NF membranes is presented in Fig. 11 (c). A digital picture of a 10 ppm feed dye solution and permeate solution after filtration is also shown in the inset. The modified membranes exhibited improved (5-fold) flux using Congo red dye feed solution due to their surface hydrophilicity enhancement. Also, both NF15 and NF20 showed an outstanding dye rejection (>99.9 %). Since the pristine membrane has also exhibited high rejection, the dye retention mechanism would be simply described herein by the size exclusion mechanism.

Finally, water permeability (L m^{-2} h^{-1} bar^{-1}) and salt and dye rejection of NF15 was compared to other state-of-the-art synthetic MM NF membranes reported in recent literature (Fig. 11 (d)). The detailed comparison is available in Table S1, SI. The literature-reported MM NF membranes have water permeability in the range of 1.4–29.7 (L m^{-2} h^{-1} bar^{-1}). Our NF15 membrane showed relatively lower permeability (1.14 L m^{-2} h^{-1} bar^{-1}) than the other MM membranes but much higher salt and dye rejections. For instance, NaCl rejection of NF15 was almost 250 % that of the best reported MM NF membranes. The well reported permeability-selectivity trade-off can explain the behavior of our QSiPD-modified NF membranes. The comparison with other MM membranes in Fig. 11 (d) suggest that our modified membranes exhibit higher selectivity, thanks to the surface effects of adding the QSiPD nanofillers, but with a compromise of membrane permeability. This still renders QSiPD a promising additive for membrane performance enhancement, but with room for further optimization of membrane properties to enhance its permeability while balancing the effect of such enhancement on its permeability. Such optimization, which takes the intended membrane application in consideration, is the topic of a follow up study. Moreover, the QSiPD-modified NF membranes have the added advantage of being resistant to bacterial growth, as discussed next.

3.5.2. *Antibacterial property*

The number of bacterial cells attached to the membrane surface has remarkably diminished in the modified UF (UF1, UF2, UF4, & UF8) and NF (NF15, & NF20) membranes (Fig. 12), in comparison to the pristine membranes (UF0 & NF0). The results also show that the antibacterial activity of the hybrid membranes progressively increased with QSiPD loading. Fig. S8, supporting information presents SEM images of the pristine (UF0) and modified (UF8) membrane after exposure to *E. coli* bacterial solution. The change in the morphological features of the attached e. coli bacterial cells may be attributed to the contact killing action of quaternized PDA. Intact *E. coli* cells were observed in pristine (UF0) membrane, while disintegrated bacterial cells were seen at the surface of modified membrane (UF8). This implies a role of QSiPD nanohybrid in granting the hybrid membranes a bactericidal effect. This antibacterial property of the modified membranes is attributed to the positively charged quaternary ammonium groups (—$N(CH_3)_3^+$) of the QSiPD nanohybrid. According to literature [25,40,50,68], such antibacterial mechanism involves the interaction of positively charged quaternary ammonium groups with the negatively charged phospholipid head groups of the *E. coli* cells. Once fixed in place, the hydrophobic portion of the quaternary ammonium groups (alkyl chain) forms micellar aggregates with the bacterial hydrophobic components that lyse bacterial cells, leading to their death. This antibacterial property of the modified membranes is essential in suppressing biofouling during UF and NF operations, giving and advantage to QSiPD modified membrane in these processes.

4. Conclusions

Mixed matrix UF and NF membranes were fabricated using QSiPD nanoparticle as an additive material. The composite membranes incorporated with hydrophilic QSiPD exhibited a significant increase in surface hydrophilicity and charge density, promoting fouling resistance properties. The water flux of the UF composite membranes was reported to be as high as ~559 L m^{-2} h^{-1} at 1 bar (for UF2). The increase in water flux was due to the synergistic effects of enhanced membrane pore structure, porosity, and hydrophilicity. Increasing the QSiPD nanohybrid content from 0 to 8 wt% reduced the membrane's irreversible fouling resistance of BSA protein from 33 % to 9.18 % (UF1), 15.2 % (UF2), 19.9 % (UF4), and 18.4 % (UF8). The hybrid NF membranes demonstrated a significant rejection rate of several salt solutions in the order of Na_2SO_4 (67%) > NaCl (47 %) > $MgSO_4$ (46 %) > $CaCl_2$(45%) for the NF15 membrane and a remarkable (>99.9 %) rejection of Congo red dye. The hybrid UF and NF membranes also showed an improved antibacterial activity against *E. coli*, most probably via contact killing mechanism. It can be concluded that QSiPD is a promising additive for membrane performance improvement with good potential in several UF and NF applications, including desalination, protein separation, and removal of dyes.

CRediT authorship contribution statement

Roqaya A. Ismail: Methodology, Investigation, Data curation, Writing - original draft. Mahendra Kumar: Supervision, Reviewing and Editing, Validation. Noman K. Khanzada: XPS analysis data curation, Navya Thomas: Reviewing and Editing, Validation. Nurshaun Sreedhar: SEM data curation. Alicia Kyoungjin An: Reviewing and Editing, Validation. Hassan A. Arafat: Conceptualization, Funding acquisition, Project administration, Writing-Reviewing and Editing, Supervision, Validation.

Declaration of competing interest

The authors declare no competing financial interest.

Acknowledgements

The research reported in this publication was supported by funding from Khalifa University through the Center for Membrane and Advanced Water Technology (CMAT), under grant no. RC2-2018-009.

Appendix A. Supplementary data

Supplementary data to this article can be found online at https://doi.org/10.1016/j.desal.2022.115954.

References

[1] R. Singh, Hybrid Membrane Systems for Water Purification Technology, Systems Design and Operation, Elsevier, Elsevier Science, Colorado Springs, USA, 2005.
[2] C.C. Ho, J.F. Su, L.P. Cheng, Fabrication of high-flux asymmetric polyethersulfone (PES) ultrafiltration membranes by nonsolvent induced phase separation process: effects of H2O contents in the dope, Polymer (Guildf) 217 (January) (2021) 123451.
[3] I. Banerjee, R.C. Pangule, R.S. Kane, Antifouling coatings: recent developments in the design of surfaces that prevent fouling by proteins, bacteria, and marine organisms, Adv. Mater. 23 (6) (2011) 690–718.
[4] G. Ye, J. Lee, F. Perreault, M. Elimelech, Controlled architecture of dual-functional block copolymer brushes on thin-film composite membranes for integrated 'Defending' and 'Attacking' strategies against biofouling, ACS Appl. Mater. Interfaces 7 (41) (Oct. 2015) 23069–23079.
[5] A. García, B. Rodríguez, D. Oztürk, M. Rosales, D.I. Diaz, A. Mautner, Incorporation of CuO nanoparticles into thin-film composite reverse osmosis membranes (TFC-RO) for antibiofouling properties, Polym. Bull. 75 (5) (2018) 2053–2069.
[6] J. Nambi Krishnan, K.R. Venkatachalam, O. Ghosh, K. Jhaveri, A. Palakodeti, N. Nair, Review of thin film nanocomposite membranes and their applications in desalination, Front. Chem. 10 (January) (2022) 1–22.
[7] X. Li, T. Cai, T.-S. Chung, Anti-fouling behavior of hyper-branched polyglycerol grafted polyethersulfone hollow fiber membranes for osmotic power generation, Environ. Sci. Technol. 48 (Jul. 2014).
[8] R. Liu, et al., Multifunctional polydopamine particles as a thermal stability modifier to prepare antifouling melt blend composite membranes, ACS Omega 6 (2) (Jan. 2021) 1352–1360.
[9] M.S.A. Saraswathi, R. Kausalya, N.J. Kaleekkal, D. Rana, A. Nagendran, BSA and humic acid separation from aqueous stream using polydopamine coated PVDF ultrafiltration membranes, J. Environ. Chem. Eng. 5 (3) (2017) 2937–2943.
[10] D. Lere Keshebo, et al., Solvent-exfoliated 2D WS2/Polyethersulfone antifouling mixed matrix ultrafiltration membrane for water treatment, ACS Appl. Polym. Mater. 2 (11) (2020) 5039–5047.
[11] M. Homayoonfal, M.R. Mehrnia, M. Shariaty-Niassar, A. Akbari, A.F. Ismail, T. Matsuura, A comparison between blending and surface deposition methods for the preparation of iron oxide/polysulfone nanocomposite membranes, Desalination 354 (2014) 125–142.
[12] R.S. Kane, P. Deschatelets, G.M. Whitesides, Kosmotropes form the basis of protein-resistant surfaces, Langmuir 19 (6) (Mar. 2003) 2388–2391.
[13] X. Wang, L. Wu, N. Li, Y. Fan, Sealing Tröger base/ZIF-8 mixed matrix membranes defects for improved gas separation performance, J. Membr. Sci. 636 (2021), 119582.
[14] Z. Yan, et al., Mussel-inspired polydopamine modification of polymeric membranes for the application of water and wastewater treatment: a review, Chem. Eng. Res. Des. 157 (2020) 195–214.
[15] H. Zhang, et al., Stability research on polydopamine and immobilized albumin on 316L stainless steel, Regen. Biomater. 3 (5) (Oct. 2016) 277–284.
[16] Q. Huang, J. Chen, M. Liu, H. Huang, X. Zhang, Y. Wei, Polydopamine-based functional materials and their applications in energy, environmental, and catalytic fields: state-of-the-art review, Chem. Eng. J. 387 (2020), 124019.
[17] L. Ni, J. Meng, X. Li, Y. Zhang, Surface coating on the polyamide TFC RO membrane for chlorine resistance and antifouling performance improvement, J. Membr. Sci. 451 (2014) 205–215.
[18] J.B. Schlenoff, Zwitteration: coating surfaces with zwitterionic functionality to reduce nonspecific adsorption, Langmuir 30 (32) (Aug. 2014) 9625–9636.
[19] M.S. Rahaman, H. Thérien-Aubin, M. Ben-Sasson, C.K. Ober, M. Nielsen, M. Elimelech, Control of biofouling on reverse osmosis polyamide membranes modified with biocidal nanoparticles and antifouling polymer brushes, J. Mater. Chem. B 2 (12) (2014) 1724–1732.
[20] Y. Liu, C. Leng, B. Chisholm, S. Stafslien, P. Majumdar, Z. Chen, Surface structures of PDMS incorporated with quaternary ammonium salts designed for antibiofouling and fouling release applications, Langmuir 29 (9) (Mar. 2013) 2897–2905.
[21] I. Banerjee, D. Mondal, J. Martin, R.S. Kane, Photoactivated antimicrobial activity of carbon nanotube–porphyrin conjugates, Langmuir 26 (22) (Nov. 2010) 17369–17374.
[22] C.H. Ho, J. Tobis, C. Sprich, R. Thomann, J.C. Tiller, Nanoseparated polymeric networks with multiple antimicrobial properties, Adv. Mater. 16 (12) (Jun. 2004) 957–961.
[23] P. Zou, W. Hartleb, K. Lienkamp, It takes walls and knights to defend a castle – synthesis of surface coatings from antimicrobial and antibiofouling polymers, J. Mater. Chem. 22 (37) (2012) 19579–19589.
[24] H. Mude, P.A. Maroju, A. Balapure, R. Ganesan, J.Ray Dutta, Quaternized polydopamine coatings for anchoring molecularly dispersed broad-spectrum antimicrobial silver salts, ACS Appl. Bio Mater. 4 (12) (Dec. 2021) 8396–8406.
[25] R.A. Ismail, M. Kumar, N. Thomas, A.K. An, H.A. Arafat, Multifunctional hybrid UF membrane from poly(ether sulfone) and quaternized polydopamine anchored reduced graphene oxide nanohybrid for water treatment, J. Membr. Sci. 639 (August) (2021), 119779.
[26] Z. Wang, X. Jiang, X. Cheng, C.H. Lau, L. Shao, Mussel-inspired hybrid coatings that transform membrane hydrophobicity into high hydrophilicity and underwater superoleophobicity for oil-in-water emulsion separation, ACS Appl. Mater. Interfaces 7 (18) (2015) 9534–9545.
[27] M. Kumar, et al., Polydopamine-coated graphene oxide nanosheets embedded in sulfonated poly(ether sulfone) hybrid UF membranes with superior antifouling properties for water treatment, Chem. Eng. J. (July) (2021), 133526.
[28] X. Tan, D. Rodrigue, A review on porous polymeric membrane preparation. Part I: production techniques with polysulfone and poly (Vinylidene Fluoride), Polymers (Basel) 11 (7) (2019) 1160.
[29] M. Kumar, N. Sreedhar, M.A. Jaoude, H.A. Arafat, High-flux, antifouling hydrophilized ultrafiltration membranes with tunable charge density combining sulfonated Poly(ether sulfone) and aminated graphene oxide nanohybrid, ACS Appl. Mater. Interfaces 12 (1) (2020) 1617–1627.
[30] R. Shevate, et al., Rapid size-based protein discrimination inside hybrid isoporous membranes, ACS Appl. Mater. Interfaces 11 (8) (2019) 8507–8516.
[31] A. Rahimpour, et al., Simultaneous improvement of antimicrobial, antifouling, and transport properties of forward osmosis membranes with immobilized highly-compatible polyrhodanine nanoparticles, Environ. Sci. Technol. 52 (9) (2018) 5246–5258.
[32] S. Lazar, et al., Mixed solvent synthesis of polydopamine nanospheres for sustainable multilayer flame retardant nanocoating, Polym. Chem. 12 (16) (2021) 2389–2396.
[33] N. Li, T. Li, X.Y. Qiao, R. Li, Y. Yao, Y.K. Gong, Universal strategy for efficient fabrication of blood compatible surfaces via polydopamine-assisted surface-initiated activators regenerated by electron transfer atom-transfer radical polymerization of zwitterions, ACS Appl. Mater. Interfaces 12 (10) (2020) 12337–12344.
[34] Z. Wang, S. Zhao, W. Zhang, C. Qi, S. Zhang, J. Li, Bio-inspired cellulose nanofiber-reinforced soy protein resin adhesives with dopamine-induced codeposition of 'water-resistant' interphases, Appl. Surf. Sci. 478 (September 2018) (2019) 441–450.
[35] A. Alkhouzaam, H. Qiblawey, Novel polysulfone ultrafiltration membranes incorporating polydopamine functionalized graphene oxide with enhanced flux and fouling resistance, J. Membr. Sci 620 (October 2020) (2021) 118900.
[36] J. Fu, et al., Adsorption of methylene blue by a high-efficiency adsorbent (polydopamine microspheres): kinetics, isotherm, thermodynamics and mechanism analysis, Chem. Eng. J. 259 (2015) 53–61.
[37] C.C. Ho, S.J. Ding, The pH-controlled nanoparticles size of polydopamine for anti-cancer drug delivery, J. Mater. Sci. Mater. Med. 24 (10) (2013) 2381–2390.
[38] F. Xu, S. Xie, R. Cao, Y.'nan Feng, C. Ren, L. Wang, Prepare poly-dopamine coated graphene@silver nanohybrid for improved surface enhanced Raman scattering detection of dyes, Sensors Actuators, B Chem. 243 (2017) 609–616.
[39] X. Guo, Engineering polydopamine-glued sandwich-like nanocomposites with antifouling and antibacterial properties for the development of advanced mixed matrix membranes, Sep. Purif. Technol. 237 (October 2019) (2020) 116326.
[40] H. Liu, et al., Preparation of a hydrophilic and antibacterial dual function ultrafiltration membrane with quaternized graphene oxide as a modifier, J. Colloid Interface Sci. 562 (2020) 182–192.
[41] Y. Ibrahim, V.S. Wadi, M. Ouda, V. Naddeo, F. Banat, S.W. Hasan, Highly selective heavy metal ions membranes combining sulfonated polyethersulfone and self-assembled manganese oxide nanosheets on positively functionalized graphene oxide nanosheets, Chem. Eng. J. 428 (July 2021) (2022) 131267.
[42] A.T. Kuvarega, N. Khumalo, D. Dlamini, B.B. Mamba, Polysulfone/N, pd co-doped TiO2 composite membranes for photocatalytic dye degradation, Sep. Purif. Technol. 191 (2018) 122–133.
[43] M. Kumar, M. Ulbricht, Novel antifouling positively charged hybrid ultrafiltration membranes for protein separation based on blends of carboxylated carbon nanotubes and aminated poly(arylene ether sulfone), J. Membr. Sci. 448 (2013) 62–73.
[44] L. Zhang, B. Chen, A. Ghaffar, X. Zhu, Nanocomposite membrane with polyethylenimine-grafted graphene oxide as a novel additive to enhance pollutant filtration performance, Environ. Sci. Technol. 52 (10) (2018) 5920–5930.
[45] M. Kumar, Z. Gholamvand, A. Morrissey, K. Nolan, M. Ulbricht, J. Lawler, Preparation and characterization of low fouling novel hybrid ultrafiltration membranes based on the blends of GO-TiO2 nanocomposite and polysulfone for humic acid removal, J. Membr. Sci. 506 (2016) 38–49.
[46] Q. Xin, et al., Enhancing the CO2 separation performance of composite membranes by the incorporation of amino acid-functionalized graphene oxide, J. Mater. Chem. A 3 (12) (2015) 6629–6641.
[47] J. Li, et al., Enhanced proton conductivity of sulfonated polysulfone membranes under low humidity via the incorporation of multifunctional graphene oxide, ACS Appl. Nano Mater. 2 (8) (2019) 4734–4743.
[48] S. Ayyaru, Y.H. Ahn, Application of sulfonic acid group functionalized graphene oxide to improve hydrophilicity, permeability, and antifouling of PVDF

nanocomposite ultrafiltration membranes, J. Membr. Sci. 525 (November 2016) (2017) 210–219.
[49] Z. Yi, C.J. Liu, L.P. Zhu, Y.Y. Xu, Ion exchange and antibiofouling properties of Poly (ether sulfone) membranes prepared by the surface immobilization of Brønsted acidic ionic liquids via double-click reactions, Langmuir 31 (29) (2015) 7970–7979.
[50] X. Zhang, Modification of microfiltration membranes by alkoxysilane polycondensation induced quaternary ammonium compounds grafting for biofouling mitigation, J. Membr. Sci. 549 (December 2017) (2018) 165–172.
[51] X. Guo, Engineering polydopamine-glued sandwich-like nanocomposites with antifouling and antibacterial properties for the development of advanced mixed matrix membranes, Sep. Purif. Technol. 237 (November 2019) (2020) 116326.
[52] R. Wang, X. Zhao, Y. Lan, L. Liu, C. Gao, In situ metal-polyphenol interfacial assembly tailored superwetting PES/SPES/MPN membranes for oil-in-water emulsion separation, J. Membr. Sci. 615 (18) (2020), 118566.
[53] Y. Mu, et al., Development of highly permeable and antifouling ultrafiltration membranes based on the synergistic effect of carboxylated polysulfone and bio-inspired co-deposition modified hydroxyapatite nanotubes, J. Colloid Interface Sci. 572 (2020) 48–61.
[54] A.K. Hołda, B. Aernouts, W. Saeys, I.F.V Vankelecom, Study of polymer concentration and evaporation time as phase inversion parameters for polysulfone-based SRNF membranes, J. Membr. Sci. 442 (2013) 196–205.
[55] L.Y. Ng, A.W. Mohammad, C.P. Leo, N. Hilal, Polymeric membranes incorporated with metal/metal oxide nanoparticles: a comprehensive review, Desalination 308 (2013) 15–33.
[56] T. van den Berg, M. Ulbricht, Polymer nanocomposite ultrafiltration membranes: the influence of polymeric additive, dispersion quality and particle modification on the integration of zinc oxide nanoparticles into polyvinylidene difluoride membranes, Membranes 10 (9) (2020).
[57] S.J. Oh, N. Kim, Y.T. Lee, Preparation and characterization of PVDF/TiO2 organic–inorganic composite membranes for fouling resistance improvement, J. Membr. Sci. 345 (1) (2009) 13–20.
[58] M. Irfan, Dual optimized sulfonated polyethersulfone and functionalized multiwall carbon tube based composites high fouling resistance membrane for protein separation, Membranes 12 (3) (2022).
[59] Z. Yi, C.-J. Liu, L.-P. Zhu, Y.-Y. Xu, Ion exchange and antibiofouling properties of Poly(ether sulfone) membranes prepared by the surface immobilization of Brønsted acidic ionic liquids via double-click reactions, Langmuir 31 (29) (Jul. 2015) 7970–7979.
[60] Z. Wang, S. Shen, L. Zhang, A. Ben Hida, G. Zhang, et al., Hydrophilic and positively charged polyvinylidene fluoride membranes for water treatment with excellent anti-oil and anti-biocontamination properties, Membranes 12 (4) (2022) 438.
[61] C.E. Lin, L.F. Fang, S.Y. Du, Z.K. Yao, B.K. Zhu, A novel positively charged nanofiltration membrane formed via simultaneous cross-linking/quaternization of poly(m-phenylene isophthalamide)/polyethyleneimine blend membrane, Sep. Purif. Technol. 212 (July 2018) (2019) 101–109.
[62] L.F. Fang, M.Y. Zhou, L. Cheng, B.K. Zhu, H. Matsuyama, S. Zhao, Positively charged nanofiltration membrane based on cross-linked polyvinyl chloride copolymer, J. Membr. Sci. 572 (October 2018) (2019) 28–37.
[63] W.R. Bowen, A.W. Mohammad, Characterization and prediction of nanofiltration membrane performance-A general assessment, Chem. Eng. Res. Des. 76 (8 A8) (1998) 885–893.
[64] W.R. Bowen, H. Mukhtar, Characterisation and prediction of separation performance of nanofiltration membranes, J. Membr. Sci. 112 (2) (1996) 263–274.
[65] Z. Mi, Z. Liu, S. Jin, D. Zhang, D. Wang, Positively charged nanofiltration membrane prepared by polydopamine deposition followed by crosslinking for high efficiency cation separation, Polym. Test. 93 (2021), 107000.
[66] O. Azzaroni, K.H.A. Lau, Layer-by-layer assemblies in nanoporous templates: nano-organized design and applications of soft nanotechnology, Soft Matter 7 (19) (2011) 8709–8724.
[67] R. Kumar, M. Ahmed, S. Ok, B. Garudachari, J.P. Thomas, Boron selective thin film composite nanofiltration membrane fabricated: via a self-assembled trimesic acid layer at a liquid-liquid interface on an ultrafiltration support, New J. Chem. 43 (9) (2019) 3874–3883.
[68] L. Mei, et al., Amino-functionalized graphene oxide for the capture and photothermal inhibition of bacteria, ACS Appl. Nano Mater. 2 (5) (2019) 2902–2908.